Nano Energy 79 (2021) 105407

Contents lists available at ScienceDirect

Nano Energy

journal homepage: http://www.elsevier.com/locate/nanoen

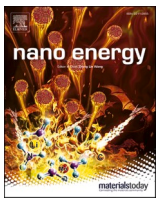

Discovering a New class of fluoride solid-electrolyte materials *via* screening the structural property of Li-ion sublattice

Bingkai Zhang [a,c,*], Jiajie Zhong [a], Yaping Zhang [b], Luyi Yang [c], Jinlong Yang [c], Shunning Li [c], Lin-Wang Wang [d], Feng Pan [c,**], Zhan Lin [a,***]

[a] Guangzhou Key Laboratory of Clean Transportation Energy Chemistry, School of Chemical Engineering and Light Industry, Guangdong University of Technology, Guangzhou, 51006, China
[b] State Key Laboratory of Environment-friendly Energy Materials, School of Materials Science and Engineering, Southwest University of Science and Technology, Mianyang, 621010, China
[c] School of Advanced Materials, Peking University Shenzhen Graduate School, Shenzhen, 518055, China
[d] Joint Center for Artificial Photosynthesis and Materials Sciences Division, Lawrence Berkeley National Laboratory, Berkeley, CA, 94720, USA

ARTICLE INFO

Keywords:
Solid-state batteries
Fluoride solid electrolyte
First-principle calculation

ABSTRACT

New structures and compositions as inorganic solid-state electrolytes (ISSEs) are needed for all-solid-state lithium batteries (ASSLBs). Here we report the theoretical discovery of three new structure types by computational identification of nearest neighbor Li–Li distance ($nR_{Li\text{-}Li}$) within Li-ion sublattice of fluorides which correlates with ISSEs ionic conductivity. This is achieved by computing Li-ions radial distribution functions and whose first peak corresponds to $nR_{Li\text{-}Li}$. Subsequent theoretical exploration of the four fluorides with small $nR_{Li\text{-}Li}$ affords three materials (Li_3MF_6 (M = Al, Sc, Ga)) with crystal structures featuring three-dimensional diffusion channels for Li-ions. The three fluoride materials exhibit very well (electro)chemical stability and high ionic conductivity. The screening method used in this work will accelerate the systematic discovery of high ionic conductivity ISSEs for use in ASSLBs and related applications.

1. Introduction

All-solid-state Li-ion batteries (ASSLBs) ASSLBs may play an important role in the future of consumer electronics and electric vehicles, as they can realize high safety and high energy density at the same time [1–5]. Typically, inorganic solid-state electrolytes (ISSEs) are incorporated in ASSLBs, primarily to overcome the volatile and flammable properties of liquid electrolytes [6–10]. Similar to organic liquid electrolytes, ISSEs needs to satisfy two important requirements: (1) high ionic conductivity and low electronic conductivity [11,12], (2) good (electro)chemical stability [13–16]. Among the members of the library, crystalline lithium fluoride (LiF) is one of the most promising coating materials for Li-metal anode, which has the widest electrochemical window so far and excellent electrochemical stability [17–23]. The strong bonding between Li and F ions on one hand contributes to the high stability of LiF, while on the other hand hampers the diffusivity of the Li-ions. It would be desirable if facile ionic diffusion can be achieved in fluoride materials without compromising their intrinsically high electrochemical stability.

It has been shown that ISSE with fast cation conduction has two different sublattices, formed by “rigid” sublattice of immobile cations and anions and “quasi-liquid” sublattice of mobile cations [24–27]. The so-called “rigid” and “quasi-liquid” arise from the ion dynamics performed by solid-state nuclear magnetic resonance (NMR) [28,29]. The “quasi-liquid” cation sublattice exhibits a unique character to facilitate ion transport in ISSEs, leading to the effect of cooperative migration of the mobile ions, which has been demonstrated in several typical ISSEs [30–32]. This concept of cation sublattice could provide a good guiding principle for the optimization of current electrolyte materials and the discovery of new high-performance ion conductors [33–36]. Moreover, current studies suggest that a strong correlation between the arrangement of Li-ion sublattice and energy barrier of Li-ion migration:

* Corresponding author. Guangzhou Key Laboratory of Clean Transportation Energy Chemistry, School of Chemical Engineering and Light Industry, Guangdong University of Technology, Guangzhou, 51006, China.
** Corresponding author.
*** Corresponding author.
E-mail addresses: zhangbk@gdut.edu.cn (B. Zhang), panfeng@pkusz.edu.cn (F. Pan), zhanlin@gdut.edu.cn (Z. Lin).

https://doi.org/10.1016/j.nanoen.2020.105407
Received 24 August 2020; Received in revised form 16 September 2020; Accepted 17 September 2020
Available online 22 September 2020
2211-2855/© 2020 Published by Elsevier Ltd.

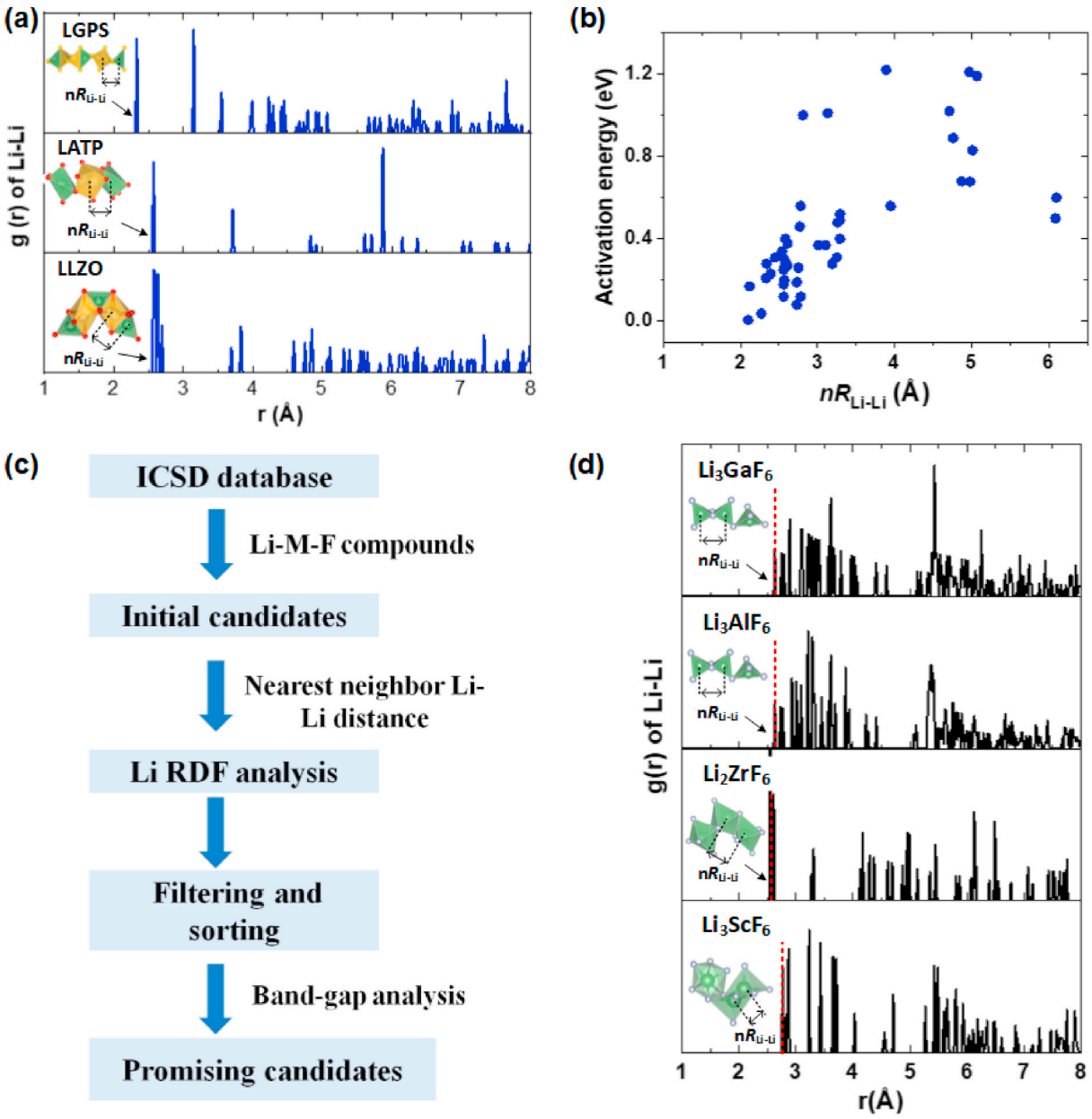

Fig. 1. (a) The Li–Li RDFs of the LGPS, LATP, and LLZO ISSEs. The insets show Li–S/O configurations and highlight the n$R_{Li\text{-}Li}$ with an arrow. (b) The correlation relationship between activation energy and n$R_{Li\text{-}Li}$ in ISSEs. The n$R_{Li\text{-}Li}$ at the range from 2 to 3 Å exhibits low activation energy for Li-ion diffusion in the whole n$R_{Li\text{-}Li}$ range. (c) Computational screening of fluoride conductors for ISSEs. (d) The Li–Li RDFs in Li-ion sublattice of Li_xMF_6. The n$R_{Li\text{-}Li}$ of these compounds (highlighted with an arrow) is around 2.7 Å, which is within the optimal range of n$R_{Li\text{-}Li}$.

compounds with interstitial Li-ions or strong Li–Li interactions exhibit low migration barriers, indicative of Li-ions cooperative migration [34, 37–39]. The best-known examples include lithium germanium thiophosphate $Li_{10}GeP_2S_{12}$ (LGPS) [30,31], NASICON-type $Li_{1.3}Al_{0.3}Ti_{1.7}(PO_4)_3$ (LATP) [32], and cubic lithium garnet $Li_7La_3Zr_2O_{12}$ (c-LLZO) [40,41]. Therefore, Li-ion sublattice could provide a unique character to optimize Li-ion transport of ISSEs.

In this work, we aimed to provide a relationship between the packing feature of Li-ion sublattice and ionic transport in ISSEs, propose the structural descriptor for Li-ion mobility, and eventually screen promising fluoride Li-ion conductors. The nearest neighbor Li–Li distance within a Li-ion sublattice can be seen as a good structural descriptor in determining intrinsic Li-ion mobility. The nearest neighbor Li–Li distance (n$R_{Li\text{-}Li}$) ranging from 2.5 to 3 Å can trigger Li-ion motion and enable fast Li-ion motion with low activation energies. Based on the n$R_{Li\text{-}Li}$ descriptor and theoretical calculations, Li_3GaF_6, Li_3AlF_6, and Li_3ScF_6 exhibit good stability and high Li-ion diffusion coefficient. The origin of the fast diffusion was elucidated by a detailed analysis of the small Li–Li distance and disordered LiF_x structural units in the fluoride materials. Density functional theory (DFT) calculations [42,43] and *ab initio* molecular dynamics (AIMD) simulations [43,44] combined with diffusivity and (electro)chemical stability analysis using the Python Materials Genomics (Pymatgen) toolkit [45–47], were employed in this work. The detailed computation methods are shown in the Supporting Information (SI).

2. Methodology section

DFT method has been very popular for calculations in solid-state physics, such as ion transport properties in crystals. For a supercell of

Table 1
Calculated structural parameters for Li_3AlF_6, Li_3GaF_6, Li_2ZrF_6, and Li_3ScF_6 crystal.

	ICSD number	Space group		a (Å)	b (Å)	c (Å)	α (°)	β (°)	γ (°)
Li_3AlF_6	252226	*C12/c1*	Theor.	14.35	8.51	9.97	90.12	94.37	90.02
			Exp.	14.23	8.40	9.88	90.00	94.10	90.00
Li_3GaF_6	409384		Theor.	14.53	8.71	10.09	89.71	94.83	89.92
			Exp.	14.37	8.57	9.99	90.00	94.80	90.00
Li_2ZrF_6	155020	*C2/c*	Theor.	10.27	8.42	5.02	89.52	117.01	89.65
			Exp.	9.65	7.53	4.99	90.00	114.90	90.00
Li_3ScF_6	415135	*P3c1*	Theosr.	8.88	8.88	9.65	89.87	89.93	120.17
			Exp.	8.78	8.78	9.52	90.00	90.00	120.00

a crystal with *n* electrons, the state function of a quantum mechanical system can be studied as a set of *n* one-electron Schrödinger-like equations. The many-electron Schrödinger equation can be very much simplified if electrons are divided in two groups: valence electrons and inner core electrons. Valence electrons were described by the plane-wave basis set and inner core electrons were kept frozen in the configuration for which the projector augment-wave approach (PAW) dataset was generated [48,49]. In this work, all structure optimization and AIMD simulations were performed using the Vienna initio Simulation Package (VASP) package with the PAW [48,49]. The exchange-correlation functional was GGA-PBE with a kinetic energy cut-off of 500 eV [50]. For structure optimization, all atomic positions and lattice parameters were allowed to relax until the forces on the atoms were less than 0.01 eV/Å and the energy difference between two self-consistent structures was less than 10^{-5} eV. K-point grids of $2 \times 2 \times 2$ were used for the supercells of Li_3AlF_6, Li_3GaF_6, Li_3ScF_6, and Li_2ZrF_6.

For AIMD calculations, the Velocity-Verlet algorithm was used to integrate Newton's equations of motion. A time step of 1.0 fs was used for integration. An NVT (or canonical) ensemble with a Nose-Hoover thermostat is employed. Only Γ-point of the k-point grid was used for all calculations. All analyses including radial distribution function, Li-ion diffusion, and phase stability were performed using the Pymatgen package developed by Ceder and co-workers [45,51]. The Li-ion diffusion coefficient (D_{Li}) was calculated from the slope of the MSD. The room temperature conductivity (σ_{Li}) was also predicted in this work. The calculation details of MSD, $D_{Li,}$ and σ_{Li} in AIMD calculations were present in SI file, and the two references (Ref. 33 and 44) also offer more information. For phase diagram and electrochemical stability, and interfacial chemical stability, we used the database consisting of DFT computed bulk energies of materials as available in the open quantum mechanical database [52,53]. The detailed calculation on phase stability of electrolytes with respect to a range of possible decomposed products, electrochemical stability of electrolytes subjected to Li chemical potentials, and interfacial stability between the electrolyte and cathodes can refer to previous papers [47,54].

3. Results and discussions

3.1. Predicted rapid Li-ion diffusion from the $nR_{Li\text{-}Li}$ descriptor

To abstract and provide insight into the (dis)order of the Li-ion sublattice, we calculated the Li-ions radial distribution functions (RDFs), in which the first peak corresponds to the nearest neighbor distance of two native lattice sites. Three compounds with high Li-ion conductivity due to cooperative migration are evaluated, LGPS, LATP, and c-LLZO, as shown in Fig. 1a. The configurations of Li-ion structure units are shown as insets of Fig. 1a. We note that the $nR_{Li\text{-}Li}$ in the three compounds is in the range of 2.4–2.7 Å. Such a short distance between the adjacent sites of the Li-ion sublattice in the above materials leads to a scenario where some of the Li-ions are squeezed into higher-energy (metastable) sites due to Li–Li repulsion interaction, thus initiating cooperative migration, that is, interstitial migration with reduced migration activation energy [54–57]. Small $nR_{Li\text{-}Li}$ is also found in other ISSEs, such as Li_3OX (X = Cl, Br) [58], Li_3N [59], Li_2CO_3 [60], and doped Li_3PO_4 [61].

To estimate the correlation of $nR_{Li\text{-}Li}$ and Li-ion mobility, we made an analysis on Li-ion migration activation energies versus $nR_{Li\text{-}Li}$ of Li-ion RDFs based on the published literatures, as shown in Fig. 1b. A full list of activation energy and $nR_{Li\text{-}Li}$ in Fig. 1b is shown in Table S1 of SI. A positive relationship between activation energy and $nR_{Li\text{-}Li}$ is found: a larger $nR_{Li\text{-}Li}$ is more likely to lead to a higher activation energy, and vice versa. Fig. 1b indicates that small $nR_{Li\text{-}Li}$ is preferred in Li-ion sublattice arrangements for Li-ion conductors owing to the low activation energy of cooperative migration. Therefore, the nearest neighbor Li–Li distance within Li-ion sublattice is an important factor in Li-ion mobility, which is applicable for Li-ion low-barrier migration in a broad range of ISSEs.

Fig. 1c shows the sequential steps of our screening process and exclusion criteria. First, we downloaded a total of 215 distinct Li-M-F fluoride compositions. Here, the fluoride materials in the inorganic crystal structure database (ICSD) for compounds contain three elements (Li, F, and M, M is cation). Next, we analyzed the Li-ion RDFs of materials using the structure analysis tools contained in Pymatgen. $nR_{Li\text{-}Li}$ is used as a descriptor for the evaluation of Li-ion mobility to exclude materials that have a $nR_{Li\text{-}Li}$ value larger than 2.8 Å. After the screening process, 11 fluoride materials are left as shown in Table S2. We note that Li_xMF_6 may be a new class of superionic conductors (Fig. 1d) as the predicted $nR_{Li\text{-}Li}$ of Li_xMF_6 is on par with state-of-the-art Li-ion conducting electrolytes. Next, we removed compounds that possess rare elements and a narrow energy band-gap (less than 3 eV) by calculating the total density of states (TDOS), thus eliminating materials that would likely to be electron conductors. In this process, Li_3AlF_6, Li_2ZrF_6, Li_3ScF_6, and Li_3GaF_6 have wide band-gap larger than 6.0 eV (as shown in Fig. S1), which suggests electrical insulation. In comparison, Li_3CrF_6, Li_3VF_6, $Li_{2.5}TiF_6$, and Li_2MnF_6, have narrow band-gap, as shown in Fig. S2. Therefore, four promising fluoride materials (Li_3AlF_6, Li_2ZrF_6, Li_3ScF_6, and Li_3GaF_6) are suggested as potential ISSEs.

3.2. Structural properties and phase stability of Li_xMF_6

The four promising fluoride materials found in this work are optimized by DFT calculations and the structural configurations are shown in Table 1 and Fig. 2a, suggesting three distinct phase structures. These crystal structures in polyhedral representation are detailed in Figs. S3–S5. For Li_3AlF_6 and Li_3GaF_6, the structures consist of an immobile framework that includes isolated MF_6 octahedrons without sharing edges or corners as well as a potential three-dimensional (3D) diffusion channel formed by interconnected LiF_x polyhedrons (see Fig. S3). For Li_2ZrF_6, the rigid structural framework is formed as isolated lagers in the *bc*-plane, which are built by the edge-sharing ZrF_8 polyhedrons (see Fig. S4). The edge-sharing LiF_6 octahedrons are sandwiched between the layers of ZrF_8 polyhedrons. Thus, the Li-ions in layered Li_2ZrF_6 may diffuse along a two-dimensional (2D) channel in *bc*-plane, from one octahedral site to another. For Li_3ScF_6, it has a framework of isolated ScF_6 octahedral units with no shared edges or corners. Li-ions are placed at distorted octahedrons which are interconnected by face-sharing and arranged in an alternating way along the conduction channels and build up a 3D Li diffusion network throughout the crystal (see Fig. S5). Overall, the crystalline structures of all four fluoride

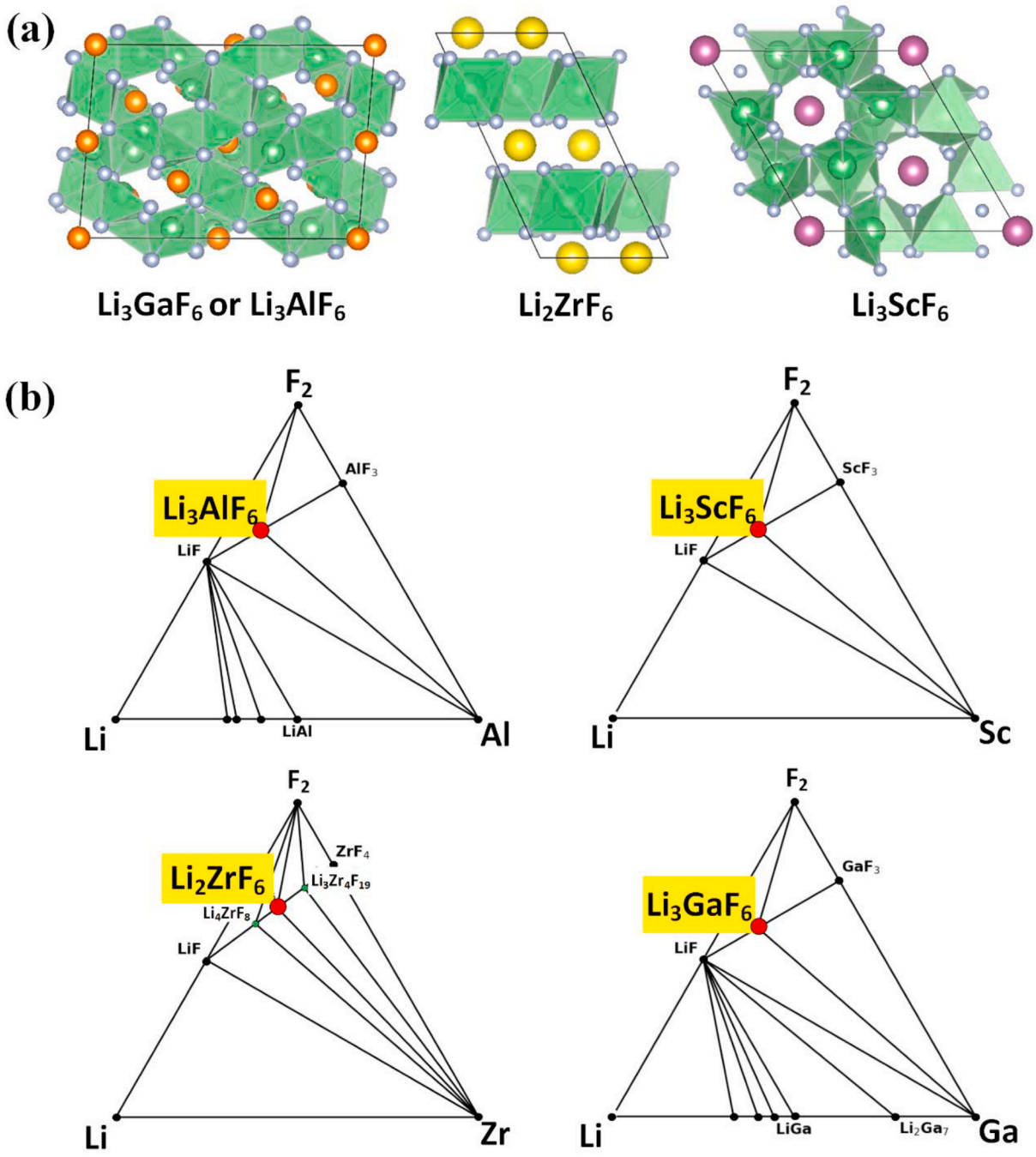

Fig. 2. (a) Crystal structure of Li_3AlF_6 (Li_3GaF_6), Li_2ZrF_6, and Li_3ScF_6 in polyhedral representation. Orange sphere, Al(Ga); yellow sphere, Zr; purple sphere, Sc; green sphere, Li; green polyhedron, LiF_x; small sky blue sphere, F. (b) Li-M-F ternary phase diagram assessing the computed stability of Li-M-F compounds. Black solid circles indicate stable phases. Red solid circles show the targeted fluoride materials. Compositions appeared in the Li-M-F phase space along with LiMF stoichiometry are shown, while the decomposition to binary phases (LiF and XF_3) is the most feasible case for Li_3AlF_6, Li_3ScF_6, and Li_3GaF_6. Li_2ZrF_6, Li_4ZrF_8, and $Li_3Zr_4F_{19}$ make up a convex hull in the LiF-ZeF_4 phase.

materials consist of LiF_x and MF_x structural units through periodic arrangements [62].

To understand the phase stability relative to their corresponding separated phases including elemental, binary, and ternary ones, we used the grand canonical linear programming method (GCLP) [63] to explore the phase diagram of Li-M-F compounds (see Fig. 2b). The GCLP writes a linear equation from a mixed or multicomponent compound into all phase equilibria and gives the combination with the lowest energy under the constraint that the coefficients for all the phase equilibria must be positive. For the four fluoride materials, the favorable combination is the decomposition of ternary Li_xMF_6 into binary LiF and MF_3 or MF_4, with the order of decomposition energy ($\Delta E = [E_{(\text{phase equilibrium})} - E_{(\text{LixMF6})}]/N_{\text{atoms}}$): Li_3GaF_6 (52 meV/atom) > Li_3AlF_6 (38 meV/atom) > Li_2ZrF_6 (13 meV/atom) > Li_3ScF_6 (1 meV/atom). These positive values suggest they are stable relative to decomposition into binary LiF and MF_3/MF_4. By comparison, we note that the decomposition energy for Li_3InCl_6 with respect to LiCl and $InCl_3$ is 14 meV/atom, which is less stable compared to Li_3GaF_6 and Li_3AlF_6, but similar to Li_2ZrF_6. And recent experiments have successfully demonstrated the air stability of Li_3InCl_6 and assembled it in a battery setup [64]. Thus, the above fluoride materials are thermodynamically stable at room temperature. It is important to note that in Li–Zr–F phase space, Li_4ZrF_8, Li_2ZrF_6, and

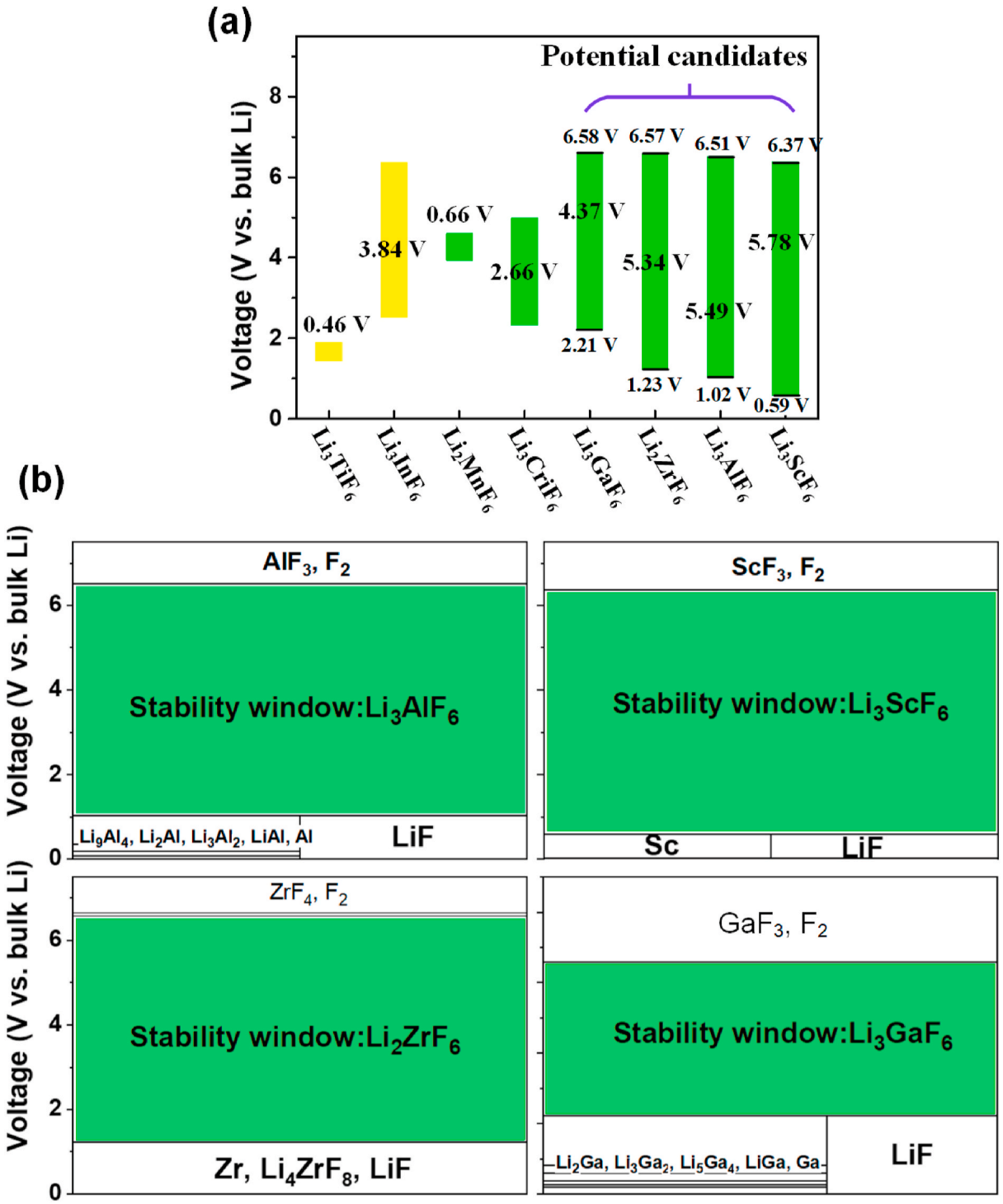

Fig. 3. (a) The electrochemical stability ranges of Li_xMF_6 fluoride electrolytes. The yellow region reflects the possible extension of the voltage window over which there is decomposition but without any metallic products. (b) The voltage profiles and phase equilibria of Li_xMF_6 upon lithiation and delithiation that determine the anodic and cathodic reactions. The stability window (green-shaded region) is determined after the energy consideration of the lithium extraction/insertion without any mutual reactions between the electrode and electrolyte.

$Li_3Zr_4F_{19}$ make up a convex hull in the LiF–ZrF_4 combination, that is, in addition to the existing Li_2ZrF_6, other possible stoichiometric ratios of LiF and ZrF_4 are within the Li–Zr–F composition diagram. To learn more about the structural stability of the four fluorides, we carried out AIMD with a canonical ensemble (NVT) at 900 K. We found that the frameworks of Li_3GaF_6, Li_3AlF_6, and Li_3ScF_6 remained stable for 100 ps of simulation, but the framework of Li_2ZrF_6 was unstable and Zr-ions migrated forming multiple Zr–F coordinations, resulting in degradation of phase structure. Thus, Li_2ZrF_6 is excluded from the further study of Li-ion migration properties.

3.3. *(electro)Chemical stability*

Achieving electrochemical stability in solid-state electrolytes is challenging while in contact with both cathode and anode due to their extreme chemical potentials and the possible chemical reactions at the

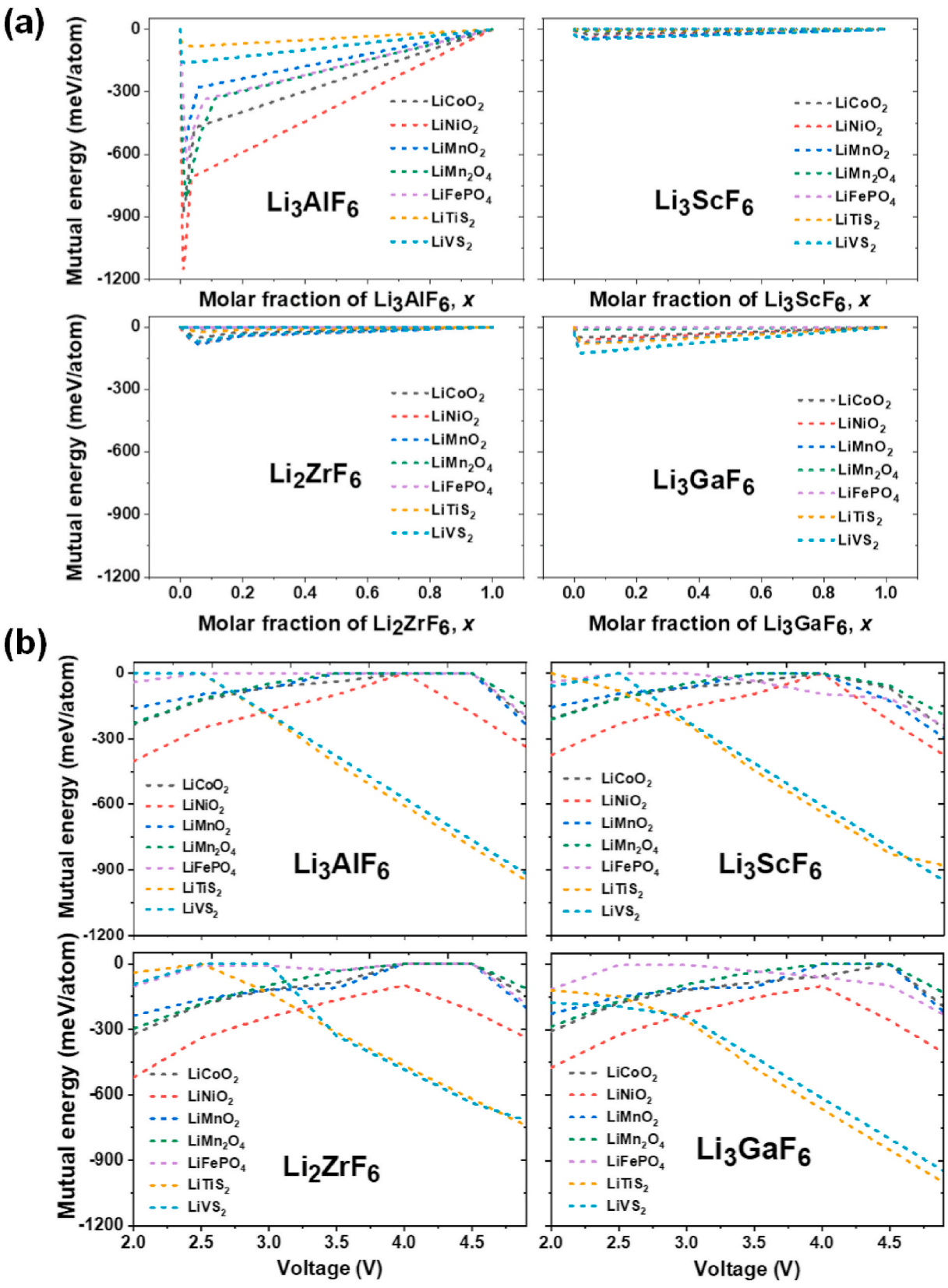

Fig. 4. (a) The calculated mutual reaction energy for the products of the interfacial reaction x·ISSEs + (1-x)·cathode → $C_{equilibrium}$ as a function of x, without any applied voltage. (b) The calculated mutual reaction energy for the products of the interfacial reaction x·ISSEs + (1-x)·cathode → $C_{equilibrium}$ as a function of voltage from 2.0 to 5.0 V vs Li/LI$^+$, x corresponds to the maximum mutual reaction energy.

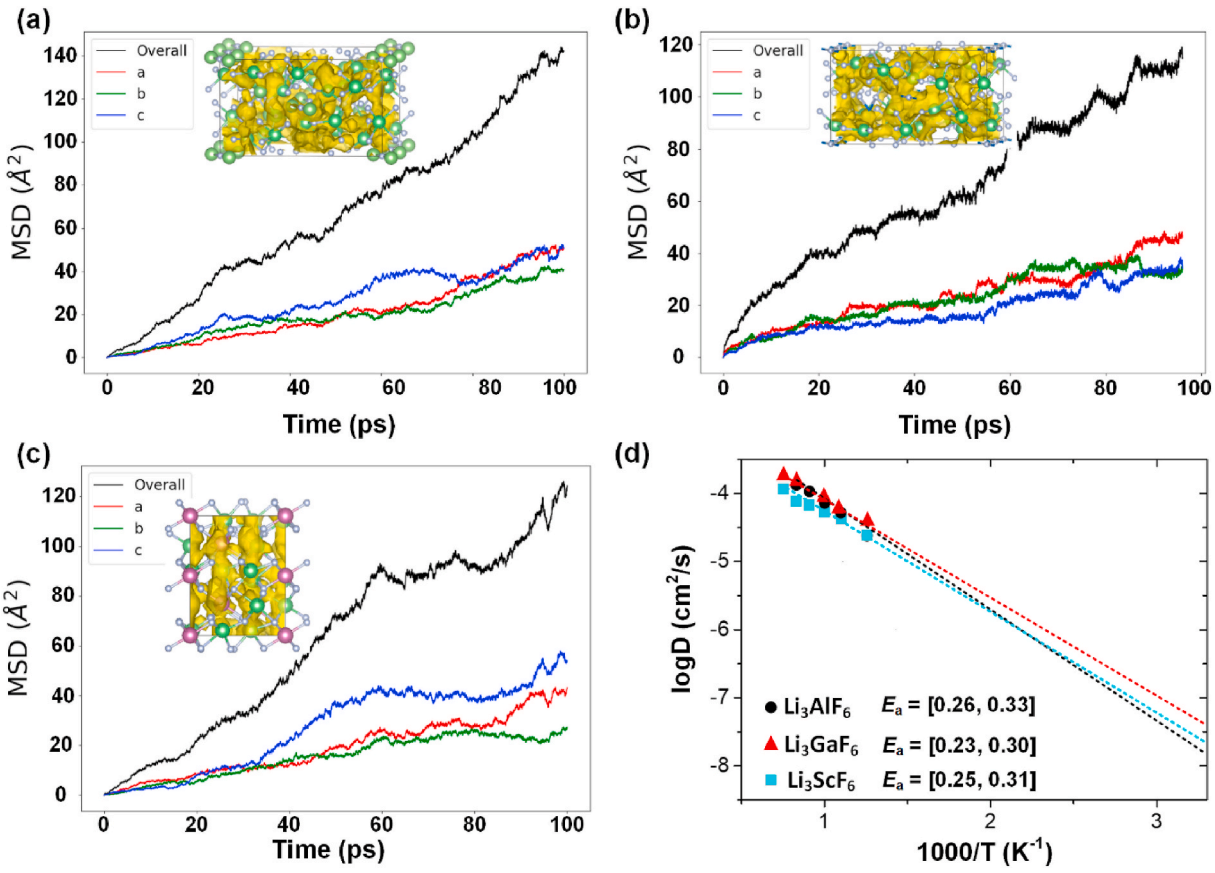

Fig. 5. (a, b and c) MSD of Li-ions along three different crystallographic directions and overall value, and probability densities (insets) obtained from the AIMD trajectory at 900 K within Li3GaF6, Li3AlF6, and Li3ScF6, respectively. (d) Li-ion diffusivity at various temperatures is fitted linearly for Li3GaF6, Li3AlF6, andLi3ScF6.

electrolyte-electrode interface [65–68]. To evaluate the interfacial stability and compatibility, we employed grand canonical phase diagrams and processed in two stages similar to the approaches adopted in previous studies [69,70]. First, we evaluated the electrochemical stability of the potential candidate by utilizing Li chemical potential (μ_{Li}) as a proxy for the voltage. The Li chemical potential is related to the applied voltage and can be determined according to the eq. $\mu_{Li}(\varphi) = \mu_{Li\text{-}metal} - e\varphi$, in which φ is the applied voltage referenced to Li metal and $\mu_{Li\text{-}metal}$ is the chemical potential of Li metal. After examining the whole window (0–5 V), we determined the stability window of fluoride materials (see Fig. 3a and b). The sequence of fluoride materials determined by their electrochemical stability window is Li_3ScF_6 (5.78 V) > Li_3AlF_6 (5.49 V) > Li_2ZrF_6 (5.34 V) > Li_3GaF_6 (4.37 V). By comparison, Li_3InF_6 can be decomposed into other compounds that are Li-ion conducting and electronically insulating (as shown in the yellow region). Li_3TiF_6, Li_2MnF_6, and Li_3CrF_6 show narrow electrochemical stability windows less than 3 V. Moreover, the fluoride materials exhibit a wider stability window compared to the sulfides. For example, the Li_3AlF_6 exhibits an anodic (cathodic) limit of 0.56 V (6.0 V) versus bulk Li, while Li_3PS_4 operates within a narrow window of 1.6–3.0 V. We also found that Li_3ScF_6 had the lowest anodic limit (as low as 0.5 V) but Li_2ZrF_6 could achieve the highest oxidation potential (up to 6 V), which was higher than all commercially available cathodes. On the anodic side, the electronically insulating and ionically conducting phase (see Fig. 3b), LiF, is formed at low voltage, which may potentially serve as a passivating interfacial phase that can act as a barrier against further solid electrolyte decomposition.

It is important to note that the computed stability window versus μ_{Li} of an electrolyte is the voltage range that the electrolyte can sustain without redox decomposition. However, this definition does not consider possible mixing reactions between electrolyte and electrode, especially considering that heating treatment or sintering is an important process in cell preparation. Next, to understand the interfacial electrochemistry of fluoride materials with cathodes, we extended the above model and consider all reaction possibilities for electrolyte/cathode interfaces: xISSEs + (1-x)Cathode → $C_{equilibrium}$, in which the $C_{equilibrium}$ is the low energy phase determined by the GCPD, and x is the stoichiometric coefficient varying from 0 to 1. Thermodynamically, the chemical stability and electrochemical stability for electrolyte/cathode interfaces are evaluated by calculating the mutual reaction energy of interfacial reactions as a function of the electrolyte ratio and voltage. The methodology to calculate mutual reaction energy can be referred to in previous studies [47,54]. The negative value of mutual reaction energies suggests an exothermic interfacial reaction. The various cathodes namely Li [M1]O_2 (M1 = Ni, Co, and Mn), Li [M2]S_2 (M2 = Ti, V), spinel $LiMn_2O_4$, and $LiFePO_4$ are herein considered (see Fig. 4a). The results in Fig. 4a show that the interfaces between Li_3AlF_6 and oxide cathodes are not thermodynamically stable at the minimum mutual reaction energies from −500 to −1100 meV per atom. For the other three fluoride compounds (Li_3ScF_6, Li_2ZrF_6, and Li_3GaF_6), the minimum mutual energies of ISSEs with cathodes are higher than −125 meV per atom. This value is close to that of LiPON with $LiCoO_2$ (−100 meV per atom) but far above that of Li_3PS_4 with $LiCoO_2$ (−406 meV per atom) [47]. The main decomposition phase equilibria are detailed in Table S3 of SI.

At applied voltages, the electrochemical stability of the fluorides with cathodes is also evaluated (see Fig. 4b). The mutual reaction energies are shown in Fig. 4b and the corresponding decomposition products are detailed in Table S4 of SI. We find that fluorides form electrochemical stable interface with sulfide ($LiTiS_2$ and $LiVS_2$) and $LiFePO_4$ at corresponding anodic and cathodic limit. However, for oxide

Table 2
Li-ion conductivity (σ) and diffusivity (D) at 300 K, activation energy (E_a) for fluorides from AIMD simulations.

	Error bar of σ (mS/cm)	*Error bar of* D (cm^2/s)	E_a (eV)
Li_3AlF_6	[1.85, 5.55]	[1.0×10^{-8}, 3.0×10^{-8}]	[0.25, 0.31]
Li_3GaF_6	[8.83, 12.36]	[5.0×10^{-8}, 7.0×10^{-8}]	[0.25, 0.32]
Li_3ScF_6	[5.11, 8.52]	[3.0×10^{-8}, 5.0×10^{-8}]	[0.26, 0.32]

cathodes, fluorides have better electrochemical stability at cathodic limit than anodic limit. This indicates that the delithiation of fluorides at high voltages will generate an additional thermodynamic driving force for the interfacial decompositions. For fluorides and oxide cathodes interfaces, the interfacial mutual reaction energies are in the range of [-550, 0] meV per atom from 2 to 5 V. In contrast, the interfacial mutual reaction energies of Li_3PS_4– $LiCoO_2$ and LLZO- $LiCoO_2$ are in the range of [-1278, −595] and [-656, −2] meV per atom from 2 to 5 V [47].

Overall, our results show that four fluoride materials exhibit large intrinsic electrochemical stability windows and good chemical stability against various cathodes. In particular, the cathodic limit for Li_xMF_6: [5.0, 6.0] V is significantly higher than sulfide ISSEs and LLZO. For future studies, it may be of interest to look into the interphase layer of fluorides with oxide cathodes by *in situ* experiments and investigate the kinetic effects on stability.

3.4. Li-ion conductivity in Li_xMF_6

Li-ion diffusivity within the fluoride framework is determined by the AIMD simulations with a total period of 100 ps. [51,71,72]. For Li_3GaF_6, Li_3AlF_6, and Li_3ScF_6, we observed an isotropic 3D network diffusion with the mean square displacement (MSD) of Li-ions in Fig. 5a–c. The 3D diffusion networks in the three materials are also proved by Li-ion probability density (insets in Fig. 5a–c) extracted from the simulated trajectories. In Fig. 5d, the diffusion coefficient (D_{Li}) values at different temperatures are extracted from the MSD analysis and use the Arrhenius relation to predict a value for ionic diffusion at room temperature. Table 2 summarizes the Li-ion conductivity, diffusivity, and activation energy for three candidates predicted. The estimated activation energy is relatively small, in the range from 0.23 to 0.33 eV, which is consistent with predictions of the nearest neighbor Li–Li distance. The sequence determined by ionic conductivity at room temperature is Li_3GaF_6 > Li_3ScF_6 > Li_3AlF_6. The ionic conductivity of three fluorides is on the order of 1.0 mS/cm at room temperature, which suggests that the three candidates have the potential to be new ion conductors.

In detail, we calculated the self (G_s (r, t)) and distinct (G_d (r, t)) parts of van Hove correlation function of Li-ions, the RDFs of Li–F from the AIMD simulations of Li_3GaF_6 (see Fig. 6a–c), Li_3AlF_6 (see Fig. S6), and Li_3ScF_6 (see Fig. S7) at 900 K. The plots of the G_s (r, t) describe how probable a Li-ion diffuses away from its original site by a distance of r after time t, and the plots of G_d (r, t) is related to the probability of finding one Li-ion when a different Li-ion is away from the original position of this Li-ion by a distance of r after time t. In G_s calculations (see Fig. 6a), the probability of finding Li-ions shifts to large r values and becomes discrete with the increase of t, and such probability is strong time dependence under different distances. Such a correlation function is typical of a superionic state. G_d results always show a significantly high probability at the proximity of $r = 0$ Å (see Fig. 6b), suggesting that Li-ions motions may be correlated. The temporal projection of G_d (r, t) at 0 and 10.5 ps (see Fig. 6c) indicates that Li-ions have left their original position and migrated to other sites. The migration of Li-ions is related to their coordination environment, known as Li-ion structure units (LiF_x). Fig. 6d shows the RDFs for Li–F interactions in Li_3GaF_6 calculated over the simulation time, and indicates two important features. First, the

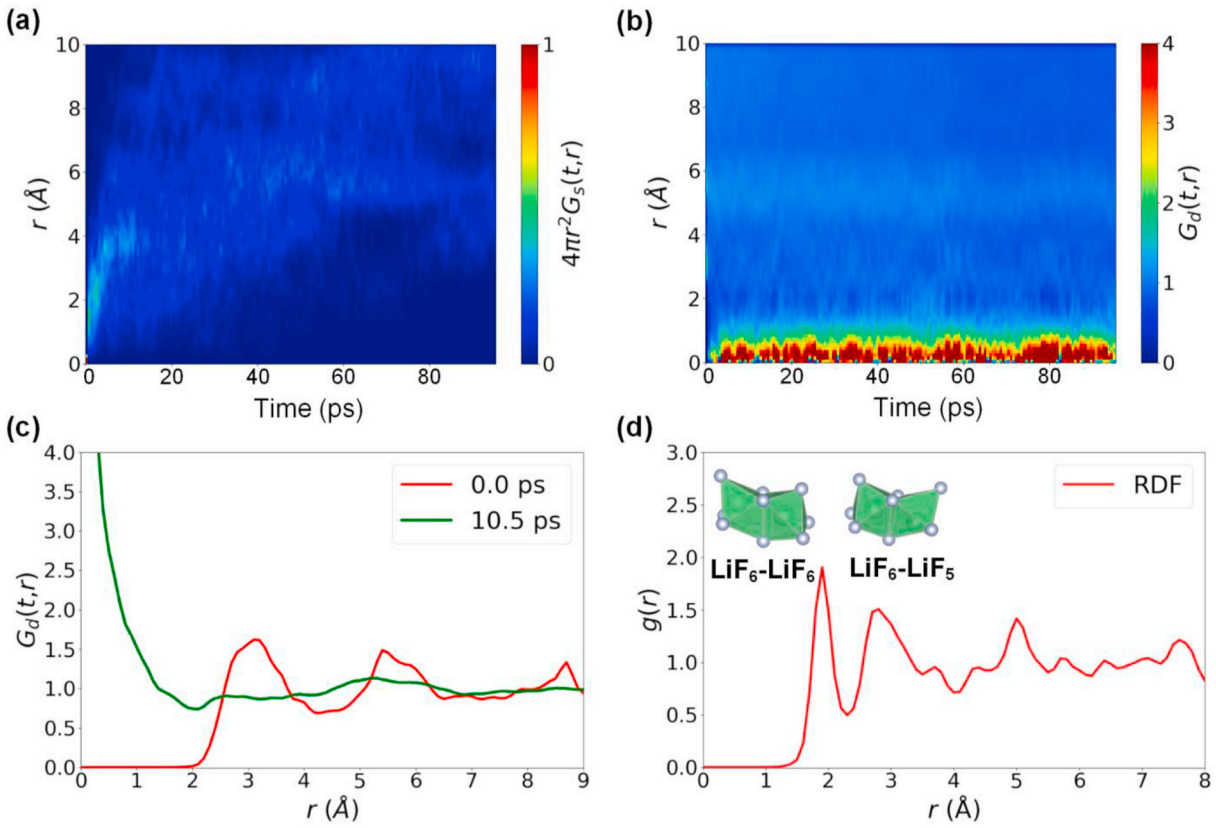

Fig. 6. (a, b) The self-part G_s and distinct-part G_d of van Hove correlation function at 900 K in Li_3GaF_6. (c) The temporal projection of distinct-part of van Hove correlation function at 900 K. (d) RDFs for Li–F interactions obtained from the simulated trajectory at 900 K in Li_3GaF_6. AIMD simulation snapshots (insets in RDFs) indicate the face-sharing LiF_x units.

weak and diffuse peaks beyond the first coordination shell indicate a great disorder and mobility of Li-ions. Second, integrating the Li-ion density up to the first coordination shell for Li–F pair in Li_xMF_6, we find there are on average 5.63 F-ions in the first coordination shell of Li-ions. We recall the initial structure at the distance of approximately 2.0 Å, whereas Li-ions exhibit 4, 5, and 6 F-ions in the first coordination shell. This suggests that great distortion of LiF_x units during simulated trajectories. The increment of the Li–F coordination sphere agrees well with the snapshots of simulated trajectories in which two adjacent LiF_6 units are generally interconnected by the face-sharing way (see insets in Fig. 6d). The pathway consisting of face-sharing interconnection octahedrons facilitates Li-ion migration with low activation energy as suggested by the previous study [73]. In summary, the AIMD simulations prove that Li-ions in three fluorides have relatively low activation energy for diffusion and a correlated motion between Li-ions, in agreement with our prediction of the bare Li-ion sublattices. Our results suggest that the method of choosing the nearest neighbor Li–Li distance to screen ISSEs is reliable.

4. Conclusion

In summary, we conducted high-throughput Li-ion radial distribution function-based screening for fluorides in search of electrochemically stable and highly conductive ISSEs. First, it was found that the correlation between Li-ion migration activation energy E_a and the nearest neighbor Li–Li distance, $nR_{Li\text{-}Li}$, can be used as a structural descriptor for the Li-ion migration activation energy, which is correlated to the ionic conductivity. The electrochemical stability using the phase diagram module contained in Pymatgen's phase diagram packages are examined. Electrolyte materials were screened based on our established exclusion criteria: (1) a $nR_{Li\text{-}Li}$ less than 3.0 Å, (2) an electronic bandgap larger than 2.0 eV, (3) an electrochemical stability window larger than 3 eV. As a result, four promising ISSEs materials with $nR_{Li\text{-}Li}$ less than 2.7 Å were proposed, and three materials were verified to have good electrochemical stability, chemical stability and high ionic conductivity. The ionic conductivity of these compounds at room temperature was predicted to be in the range of [1,10] mS/cm, which was on par with currently reported garnet-type materials. Moreover, their electrochemical stability windows were in the range of [4.37, 5.78] V.

For ASSLBs technology implications, the Li_3AlF_6, Li_3GaF_6, and Li_2ZrF_6 may be promising ISSEs candidates. For future studies, it may be of interest to experimentally verify their electrochemical stability and conductivity. Besides, we suggest that the use of $nR_{Li\text{-}Li}$ descriptor may be a universal strategy to screen high ionic conductivity ISSEs materials. Similar screening studies of the current work on chloride and bromide materials may result in more promising ISSEs candidates.

Declaration of competing interest

The authors declare that they have no known competing financial interests or personal relationships that could have appeared to influence the work reported in this paper.

Acknowledgments

This work was supported by National Key R&D Program of China (2016YFB0700600), Soft Science Research Project of Guangdong Province (No. 2017B030301013). Wang was supported by the Assistant Secretary for Energy Efficiency and Renewal Energy of the U.S. Department of Energy under the Battery Materials Research (BMR) program.

Appendix A. Supplementary data

Supplementary data to this article can be found online at https://doi.org/10.1016/j.nanoen.2020.105407.

References

[1] B. Zhang, R. Tan, L. Yang, J. Zheng, K. Zhang, S. Mo, Z. Lin, F. Pan, Energy Storage Mater 10 (2018) 139–159.
[2] Z. Lin, Z. Liu, N.J. Dudney, C. Liang, ACS Nano 7 (2013) 2829–2833.
[3] Z. Jiang, H. Xie, S. Wang, X. Song, X. Yao, H. Wang, Adv. Energy Mater. 8 (2018) 1801433.
[4] J. Xiang, L. Yang, L. Yuan, K. Yuan, Y. Zhang, Y. Huang, J. Lin, F. Pan, Y. Huang, Joule 3 (2019) 2334–2363.
[5] C. Xu, Y. Yang, H. Wang, Y. Li, R. Tan, X. Duan, D. Wu, M. Zhuo, J. Ma, B. Xu, Chem. Asian J. (2020), https://doi.org/10.1002/asia.202000851.
[6] S. Wang, Q. Bai, A.M. Nolan, Y. Liu, S. Gong, Q. Sun, Y. Mo, Angew. Chem. Int. Ed. 24 (2019) 8039–8043.
[7] X. Li, J. Liang, N. Chen, J. Luo, X. Sun, Angew. Chem. Int. Ed. 131 (2019) 16579–16584.
[8] F. Lu, Y. Pang, M. Zhu, F. Han, J. Yang, F. Fang, D. Sun, S. Zheng, C. Wang, Adv. Funct. Mater. 29 (2019) 1809219.
[9] Y. Pang, X. Wang, X. Shi, F. Xu, L. Sun, J. Yang, S. Zheng, Adv. Energy Mater. 10 (2020) 1902795.
[10] Z.-J. He, L.-Z. Fan, Rare Met. 37 (2018) 488–496.
[11] Y. Song, L. Yang, L. Tao, Q. Zhao, Z. Wang, Y. Cui, H. Liu, Y. Lin, F. Pan, J. Mater. Chem. A 7 (2019) 22898–22902.
[12] Y. Song, L. Yang, W. Zhao, Z. Wang, Y. Zhao, Z. Wang, Q. Zhao, H. Liu, F. Pan, Adv. Energy Mater. 9 (2019) 1900671.
[13] L. Yang, Y. Song, H. Liu, Z. Wang, K. Yang, Q. Zhao, Y. Cui, J. Wen, W. Luo, F. Pan, Small Methods 4 (2020) 1900751.
[14] X.-Q. Zhang, X. Chen, X.-B. Cheng, B.-Q. Li, X. Shen, C. Yan, J.-Q. Huang, Q. Zhang, Angew. Chem. Int. Ed. 130 (2018) 16885–16889.
[15] Y. Huang, B. Chen, J. Duan, F. Yang, Y. Huang, Angew. Chem. Int. Ed. 59 (2019) 3699–3704.
[16] J. Hu, K. Chen, C. Li, Energy Storage Mater 28 (2020) 37–46.
[17] Y. Yuan, F. Wu, Y. Bai, Y. Li, G. Chen, Z. Wang, C. Wu, Energy Storage Mater 16 (2019) 411–418.
[18] J. Ko, Y.S. Yoon, Ceram. Int. 45 (2019) 30–49.
[19] J. Zhao, L. Liao, F. Shi, T. Lei, G. Chen, A. Pei, J. Sun, K. Yan, G. Zhou, J. Xie, C. Liu, Y. Li, Z. Liang, Z. Bao, Y. Cui, J. Am. Chem. Soc. 139 (2017) 11550–11558.
[20] J. Xie, L. Liao, Y. Gong, Y. Li, F. Shi, A. Pei, J. Sun, R. Zhang, B. Kong, R. Subbaraman, J. Christensen and Y. Cui, 3 (2017) eaao3170.
[21] Z. Peng, N. Zhao, Z. Zhang, H. Wan, H. Lin, M. Liu, C. Shen, H. He, X. Guo, J.-G. Zhang, D. Wang, Nano Energy 39 (2017) 662–672.
[22] B. Zhang, Z. Lin, H. Chen, L.-W. Wang, F. Pan, J. Mater. Chem. A 8 (2020) 2613–2617.
[23] X. Shi, Y. Pang, B. Wang, H. Sun, X. Wang, Y. Li, J. Yang, H.W. Li, S. Zheng, Mater. Today Nano 10 (2020) 100079.
[24] L. Strock, Z Phys Chem-Abt B (1934) 441–459.
[25] S.-H. Bo, Y. Wang, J.C. Kim, W.D. Richards, G. Ceder, Chem. Mater. 28 (2016) 252–258.
[26] P. Canepa, S.-H. Bo, G. Sai Gautam, B. Key, W.D. Richards, T. Shi, Y. Tian, Y. Wang, J. Li, G. Ceder, Nat. Commun. 8 (2017) 1759.
[27] Q. Zhao, L. Pan, Y.-J. Li, L.-Q. Chen, S.-Q. Shi, Rare Met. 37 (2018) 497–503.
[28] A. Kuhn, S. Narayanan, L. Spencer, G. Goward, V. Thangadurai, M. Wilkening, Phys. Rev. B 83 (2011), 094302.
[29] A. Kuhn, M. Kunze, P. Sreeraj, H.D. Wiemhöfer, V. Thangadurai, M. Wilkening, P. Heitjans, Solid State Nucl. Magn. Reson. 42 (2012) 2–8.
[30] Y. Sun, K. Suzuki, S. Hori, M. Hirayama, R. Kanno, Chem. Mater. 29 (2017) 5858–5864.
[31] N. Kamaya, K. Homma, Y. Yamakawa, M. Hirayama, R. Kanno, M. Yonemura, T. Kamiyama, Y. Kato, S. Hama, K. Kawamoto, A. Mitsui, Nat. Mater. 10 (2011) 682–686.
[32] B. Lang, B. Ziebarth, C. Elsässer, Chem. Mater. 27 (2015) 5040–5048.
[33] X. He, Q. Bai, Y. Liu, A.M. Nolan, C. Ling, Y. Mo, Adv. Energy Mater. 9 (2019) 1902078.
[34] X. He, Y. Zhu, Y. Mo, Nat. Commun. 8 (2017) 15893.
[35] R. Xiao, H. Li, L. Chen, Sci. Rep. 5 (2015) 14227.
[36] R. Xiao, H. Li, L. Chen, J. Materiomics 1 (2015) 325–332.
[37] Y. Chen, E. Rangasamy, C. Liang, K. An, Chem. Mater. 27 (2015) 5491–5494.
[38] Z. Zhang, Z. Zou, K. Kaup, R. Xiao, S. Shi, M. Avdeev, Y.S. Hu, D. Wang, B. He, H. Li, Adv. Energy Mater. 9 (2019) 1902373.
[39] Y. Gao, A.M. Nolan, P. Du, Y. Wu, C. Yang, Q. Chen, Y. Mo, S.-H. Bo, Chem. Rev. 120 (2020) 5954–6008.
[40] R. Jalem, M.J.D. Rushton, W. Manalastas, M. Nakayama, T. Kasuga, J.A. Kilner, R. W. Grimes, Chem. Mater. 27 (2015) 2821–2831.
[41] M. Xu, M.S. Park, J.M. Lee, T.Y. Kim, Y.S. Park, E. Ma, Phys. Rev. B 85 (2012), 052301.
[42] H. Xu, Y. Yu, Z. Wang, G. Shao, Energ. Environ. Mater. 2 (2019) 234–250.
[43] S. Shi, J. Gao, Y. Liu, Y. Zhao, Q. Wu, W. Ju, C. Ouyang, R. Xiao, Chin. Phys. B 25 (2016), 018212.
[44] X. He, Y. Zhu, A. Epstein, Y. Mo, NPJ Comput. Mater. 4 (2018) 18.
[45] S.P. Ong, W.D. Richards, A. Jain, G. Hautier, M. Kocher, S. Cholia, D. Gunter, V. L. Chevrier, K.A. Persson, G. Ceder, Comput. Mater. Sci. 68 (2013) 314–319.
[46] S.P. Ong, Y. Mo, W.D. Richards, L. Miara, H.S. Lee, G. Ceder, Energ. Environ. Mater. 6 (2013) 148–156.
[47] Y. Zhu, X. He, Y. Mo, J. Mater. Chem. A 4 (2015) 3253–3266.
[48] P.E. Blöchl, Phys. Rev. B 50 (1994) 17953–17979.
[49] G. Kresse, J. Furthmüller, Phys. Rev. B 54 (1996) 11169–11186.
[50] J.P. Perdew, K. Burke, M. Ernzerhof, Phys. Rev. Lett. 77 (1996) 3865–3868.

[51] Z. Deng, Z. Zhu, I.-H. Chu, S.P. Ong, Chem. Mater. 29 (2017) 281–288.
[52] S. Kirklin, J.E. Saal, B. Meredig, A. Thompson, J.W. Doak, M. Aykol, S. Rühl, C. Wolverton, NPJ Comput. Mater. 1 (2015) 15010.
[53] S. Banerjee, X. Zhang, L.-W. Wang, Chem. Mater. 31 (2019) 7265–7276.
[54] B. Zhang, Z. Lin, L.-W. Wang, F. Pan, ACS Appl. Mater. Interfaces 12 (2020) 6007–6014.
[55] B. Zhang, Z. Lin, H. Dong, L.-W. Wang, F. Pan, J. Mater. Chem. A 8 (2020) 342–348.
[56] B. Zhang, M. Weng, Z. Lin, Y. Feng, L. Yang, L.-W. Wang, F. Pan, Small 16 (2020) 1906374.
[57] B. Zhang, L. Yang, L.-W. Wang, F. Pan, Nano Energy 62 (2019) 844–852.
[58] A. Emly, E. Kioupakis, A. Van der Ven, Chem. Mater. 25 (2013) 4663–4670.
[59] W. Li, G. Wu, C.M. Araújo, R.H. Scheicher, A. Blomqvist, R. Ahuja, Z. Xiong, Y. Feng, P. Chen, Energ. Environ. Mater. 3 (2010) 1524–1530.
[60] S. Shi, P. Lu, Z. Liu, Y. Qi, L.G. Hector, H. Li, S.J. Harris, J. Am. Chem. Soc. 134 (2012) 15476–15487.
[61] Y. Deng, C. Eames, J.-N. Chotard, F. Lalère, V. Seznec, S. Emge, O. Pecher, C. P. Grey, C. Masquelier, M.S. Islam, J. Am. Chem. Soc. 137 (2015) 9136–9145.
[62] J. Zheng, Y. Ye, F. Pan, Nat. Sci. Rev. 7 (2019) 242–245.
[63] S. Kirklin, B. Meredig, C. Wolverton, Adv. Energy Mater. 3 (2013) 252–262.
[64] X. Li, J. Liang, J. Luo, M. Norouzi Banis, C. Wang, W. Li, S. Deng, C. Yu, F. Zhao, Y. Hu, T.-K. Sham, L. Zhang, S. Zhao, S. Lu, H. Huang, R. Li, K.R. Adair, X. Sun, Energ. Environ. Mater. 12 (2019) 2665–2671.
[65] Y. Xiao, Y. Wang, S.-H. Bo, J.C. Kim, L.J. Miara, G. Ceder, Nat. Rev. Mater. 5 (2020) 105–126.
[66] Y. Tian, T. Shi, W.D. Richards, J. Li, J.C. Kim, S.-H. Bo, G. Ceder, Energ. Environ. Mater. 10 (2017) 1150–1166.
[67] B.R. Shin, Y.J. Nam, D.Y. Oh, D.H. Kim, J.W. Kim, Y.S. Jung, Electrochim. Acta 146 (2014) 395–402.
[68] F. Han, Y. Zhu, X. He, Y. Mo, C. Wang, Adv. Energy Mater. 6 (2016) 1501590.
[69] Y. Zhu, X. He, Y. Mo, ACS Appl. Mater. Interfaces 7 (2015) 23685–23693.
[70] W.D. Richards, L.J. Miara, Y. Wang, J.C. Kim, G. Ceder, Chem. Mater. 28 (2016) 266–273.
[71] Z. Zhu, I.-H. Chu, Z. Deng, S.P. Ong, Chem. Mater. 27 (2015) 8318–8325.
[72] Z. Zhu, I.-H. Chu, S.P. Ong, Chem. Mater. 29 (2017) 2474–2484.
[73] Y. Wang, W.D. Richards, S.P. Ong, L.J. Miara, J.C. Kim, Y. Mo, G. Ceder, Nat. Mater. 14 (2015) 1026–1031.

Dr. Bingkai Zhang received the Ph.D. degree from Huazhong University of Science and Technology, China, in 2014. He was a postdoc of School of Advanced Materials, Peking University Shenzhen Graduate School, Shenzhen, China, from 2014 to 2019. From 2017 to 2019, he acted as a visiting scholar in Materials Sciences Division (MSD), Lawrence Berkeley National Laboratory, US. Since June 2019, he has been an associate professor of School of Chemical Engineering and Light Industry, Guangdong University of Technology, China. His research interests are on research and development of new materials for energy conversion and storage, and characterization of materials using first-principle calculation and molecular dynamics.

Jiajie Zhong received his B.S. degree in Chemistry from Dongguan University of Technology in 2020. He is pursuing his M.S. degree in the School of Chemical Engineering and Light Industry, Guangdong University of Technology. His research interests focus on solid-state electrolytes in all solid-state lithium batteries.

Prof. Yaping Zhang received her Ph.D. degree in Department of Chemistry from University of Science and Technology of China in 2006. Currently she is a professor from School of Materials Science and Engineering in Southwest University of Science and Technology. Her research interest mainly focuses on new energy, including lithium-ion batteries, lithium-sulfur batteries and all-vanadium redox flow batteries.

Dr. Luyi Yang received his B.S. degree from the Department of Chemistry at Xiamen University (China) in 2010, and earned Ph.D. degree from the School of Chemistry at Southampton University (U.K.) in 2015 under the supervision of Prof. John Owen. Dr. Yang is currently a researcher at the School of Advanced Materials, Peking University Shenzhen Graduate School. His research interests mainly focus on the investigation of key materials in lithium batteries including solid-state electrolytes, layered oxide cathode materials and binders for Si anodes.

Dr. Jinlong Yang is an assistant professor at Shenzhen University. He received his Ph.D. degree in 2014 from Wuhan University of Technology, China. He was a postdoctoral scholar from 2014 to 2018 at Peking University, China and from 2018 to 2020 at Stanford University, USA. His research interests include: advanced energy materials (for battery and catalysis), nanotechnology and electrochemistry.

Dr. Shunning Li received his B.E. degree in 2013 and Ph.D. degree in 2018 from School of Materials Science and Engineering, Tsinghua University, China. Currently, he is an assistant research fellow at the School of Advanced Materials, Peking University, Shenzhen Graduate School, China. His research interest focuses on the first-principles design of energy storage materials and heterogeneous catalysts.

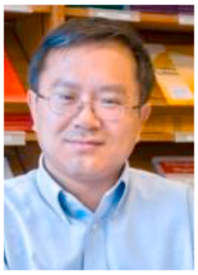

Dr. Lin-Wang Wang is a Senior Staff Scientist at Lawrence Berkeley National Laboratory. Dr. Wang has 25 years of experience in large scale electronic structure calculations. Worked with Alex Zunger, he invented the folded spectrum method. He developed a linear combination of bulk bands (LCBB) method for semiconductor heterostructure electronic structure calculations, generalized moments method, a popular parallel total energy plane wave pseudopotential program (PEtot), and a linear scaling three dimensional fragment method (LS3DF). He invented a charge patching method, which enables the *ab initio* accuracy thousand atom calculations for nanosystems. Recently, he developed a new algorithm for real-time time-dependent DFT calculations which accelerates the traditional algorithms by hundreds of times.

Prof. Feng Pan, Chair-Professor, Founding Dean of School of Advanced Materials, Peking University Shenzhen Graduate School, Director of National Center of Electric Vehicle Power Battery and Materials for International Research, got B.S. from Dept. Chemistry, Peking University in1985 and PhD from Dept. of P&A Chemistry, University of Strathclyde, Glasgow, UK, with "Patrick D. Ritchie Prize" for the best Ph.D. in 1994. Prof. Pan has been engaged in fundamental research and product development of novel energy conversion and storage materials & devices. As Chief Scientist, Prof. Pan led 12 entities to win National Key project of Material Genomic Engineering for Solid State Li-ion Battery in China in 2016. He has been selected as one of the 2018 winner of ECS Battery Division Technology Award.

Prof. Zhan Lin obtained his Ph.D. degree from North Carolina State University in 2010. After that, he worked as a post-doctoral research associate in Oak Ridge National Laboratory and University of California-Berkeley from 2011 to 2013. He returned to China in 2014, and now he is a full professor in School of Chemical Engineering and Light Industry at Guangdong University of Technology. His research mainly focuses on advanced materials for energy storage and conversion.